Spin-wave analysis of the transverse-field Ising model on the checkerboard lattice

Louis-Paul Henry,[1] Peter C. W. Holdsworth,[1] Frédéric Mila,[2] and Tommaso Roscilde[1]

[1]*Laboratoire de Physique, CNRS UMR 5672, Ecole Normale Supérieure de Lyon, Université de Lyon,
46 Allée d'Italie, Lyon, FR-69364 France*

[2]*Institut de Théorie des Phenomènes Physique, Ecole Polytechnique Fédérale de Lausanne (EPFL), CH-1015 Lausanne, Switzerland*

The ground-state properties of the $S = 1/2$ transverse-field Ising model on the checkerboard lattice are studied using linear spin-wave theory. We consider the general case of different couplings between nearest neighbors (J_1) and next-to-nearest neighbors (J_2). In zero field, the system displays a large degeneracy of the ground state, which is exponential in the system size (for $J_1 = J_2$) or in the system's linear dimensions (for $J_2 > J_1$). Quantum fluctuations induced by a transverse field are found to be unable to lift this degeneracy in favor of a classically ordered state at the harmonic level. This remarkable fact suggests that a quantum-disordered ground state can be instead promoted when nonlinear fluctuations are accounted for, in agreement with existing results for the isotropic case $J_1 = J_2$. Moreover, spin-wave theory shows sizable regions of instability, which are further candidates for quantum-disordered behavior.

I. INTRODUCTION

Frustrated quantum magnets represent one of the richest playgrounds to investigate quantum collective phenomena.[1] Indeed, known models of frustrated quantum magnets might admit quantum ground states without any classical counterpart, such as valence-bond crystals, or resonating-valence-bond spin liquids.[2] Most of the investigations have focused on Heisenberg antiferromagnets due to their relevance to real compounds, although the lack of well-controlled analytical or numerical approaches for the bulk properties of these systems still leaves the question open on the true nature of their ground state.[3] On the other hand, quantum-disordered ground states have been shown to emerge in models with strongly anisotropic interactions (in spin space and/or in real space), which appear to provide the first controlled realizations of quantum spin liquids with a topological nature.[4–7] Some of these systems are related to quantum dimer models,[8,9] which have provided the first known examples of quantum spin-liquid ground states.[10]

In this class of anisotropic systems, a special role is played by frustrated quantum Ising models, namely, Ising systems enriched with quantum fluctuations, coming either from an exchange coupling in the transverse spin components or from a transverse magnetic field.[11,12] In the absence of quantum fluctuations, Ising models on frustrated lattices have generally a *classical* spin-liquid nature, namely, they exhibit an exponential degeneracy of the ground state, as it is the case for the Ising antiferromagnet on the triangular lattice, kagome lattice, checkerboard lattice, pyrochlore lattice, etc., with, however, correlations that can be long ranged, algebraic, or short ranged. The effect of quantum fluctuations is in general that of lifting the large degeneracy of ground states, leading either to the emergence of an ordered ground state (as, e.g., in the case of the triangular lattice[11]) or to a ground state with novel spin-liquid properties (as it appears to be the case for the pyrochlore lattice[4,6]). In this study, we focus on the Ising antiferromagnet on the checkerboard lattice, which represents a fundamental model of frustrated magnetism in two dimensions. Indeed, in the case of spatially isotropic interactions, the ground-state properties of the system are

equivalent to those of the unbiased six-vertex model, also known as square ice.[13] The effect of quantum fluctuations on such a system has been the subject of several recent investigations[11,14–18] focusing particularly on the limit of weak quantum fluctuations, treated within degenerate perturbation theory.

In this study, we adopt a different strategy, which allows us to treat arbitrarily strong quantum fluctuations in a generalized version of square ice. We investigate the $S = 1/2$ Ising model on the checkerboard lattice with different couplings along the coordinate axes (J_1) and along the diagonals (J_2), as shown in Fig. 1. The anisotropy in the couplings allows us to introduce a bias in the vertex weights of the corresponding vertex model, reducing the degeneracy to exponential in the linear dimensions of the system ($J_2 > J_1$), or even to a finite value (for $J_1 > J_2$). The application of a transverse field allows us therefore to investigate the effect of quantum fluctuations on a classical manifold of states with variable degeneracy. Quantum fluctuations are investigated via linear spin-wave theory, accounting for the harmonic fluctuations around the classical ground state. Albeit limited to the harmonic approximation, such an approach allows for investigation of arbitrarily strong fields, and its breakdown signals the candidate regions in the phase diagram where novel quantum-disordered behavior can be expected. On the side $J_2 > J_1$, the infinite degeneracy of the ground state would *a priori* make the spin-wave analysis impossible, given the exceedingly large number of possible classical reference states. In fact, we demonstrate that the spin-wave spectrum does *not* depend on the particular classical ground state chosen as a reference. This implies that the spectrum of linear excitations is defined unambiguously in the $J_2 > J_1$ region; this situation persists also in the isotropic case of square ice $J_1 = J_2$, for which the lowest branch of the excitation spectrum is a flat band. But, this implies as well that the classical degeneracy remains unaltered in the presence of harmonic quantum fluctuations, which means that only nonlinear quantum fluctuations can lift the degeneracy, a situation previously encountered in a number of frustrated magnets.[19–25] Moreover, harmonic quantum fluctuations
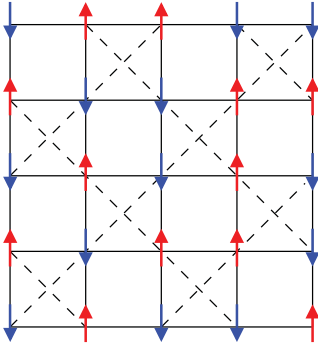
FIG. 1. (Color online) Checkerboard lattice. Full lines represent couplings with strength J_1, dashed lines represent couplings with strength J_2.

triggered by a sufficiently strong field are found to reverse the classical hierarchy of ordered states close to the isotropic ($J_1 = J_2$) limit, suggesting that anharmonic fluctuations might destabilize the classical order completely. Finally, the classical order parameter is found to be completely washed out by quantum fluctuations for strong fields close to the classical polarization transition, and for couplings close to the isotropic case. We can therefore conclude that the transverse-field Ising model (TFIM) on the checkerboard lattice can harbor quantum-disordered phases for strong frustration and fields, and that nonlinear quantum fluctuations are expected to play a major role in the case of extensive degeneracy of the ground state.

The paper is structured as follows: Section II describes the model, its behavior in zero applied field, and the classical behavior in a transverse field; Sec. III reviews known results on quantum square ice from degenerate perturbation theory and numerics; Sec. IV describes linear spin-wave theory as applied to the various regimes of the checkerboard lattice TFIM; Sec. V discusses the phase diagram emerging from spin-wave theory; and finally conclusions are drawn in Sec. VI, along with a discussion about physical realizations. The general framework of spin-wave theory for the TFIM on arbitrary lattices is presented in Appendix A, while the spin-wave observables for the checkerboard lattice are discussed in Appendix B.

II. CLASSICAL BEHAVIOR OF THE TRANSVERSE-FIELD ISING MODEL ON THE CHECKERBOARD LATTICE

A. Model Hamiltonian and ground-state properties in zero field

The Hamiltonian of the TFIM on the checkerboard lattice reads as

$$\mathcal{H} = J_1 \sum_{\langle i,j \rangle} S_i^z S_j^z + J_2 \sum_{\langle\langle i,j \rangle\rangle} S_i^z S_j^z - \Gamma \sum_i S_i^x, \qquad (1)$$

where S_i are quantum spins of length S, satisfying $|S_i|^2 = S(S+1)$ and $[S_i^\alpha, S_i^\beta] = i\varepsilon_{\alpha\beta\gamma}S_i^\gamma$. The first sum in Eq. (1) runs over the nearest-neighbor bonds of a square lattice, while the second sum runs over the next-to-nearest-neighbor (diagonal) bonds on a staggered array of plaquettes (see Fig. 1). We consider here frustrated antiferromagnetic couplings J_1, $J_2 > 0$. Γ is a transverse magnetic field, introducing quantum fluctuations in the system. As we will see in the following

section, in zero field, the ground-state properties of the above model are equivalent to those of an m-vertex model with $m = 2$, 4 or 6 depending on the Hamiltonian parameters. Motivated by this equivalence, in the following we will indicate as *vertices* (denoted by $\boxtimes$) the squares with additional diagonal J_2 couplings, and as *plaquettes* (denoted by $\square$) the squares without diagonal couplings.

When $\Gamma = 0$, we can easily rewrite the Hamiltonian in the following form:

$$\mathcal{H} = J_2 h_{\text{ice}} + (J_1 - J_2) \sum_{\langle i,j \rangle} S_i^z S_j^z \qquad (2)$$

if $J_1 > J_2$, and

$$\mathcal{H} = J_1 h_{\text{ice}} + (J_2 - J_1) \sum_{\langle\langle i,j \rangle\rangle} S_i^z S_j^z \qquad (3)$$

if $J_2 > J_1$, where we have introduced the square-ice Hamiltonian

$$h_{\text{ice}} = \sum_{\boxtimes} \left[\left(\sum_{i \in \boxtimes} S_i^z \right)^2 - 4 \sum_{i \in \boxtimes} \left(S_i^z \right)^2 \right]. \qquad (4)$$

With this choice, the ground state is identified in two steps: (1) first, one needs to impose on each spin the constraint that $S_i^z = \pm S$, and on each vertex the zero-magnetization constraint $M_{\boxtimes} = \sum_{i \in \boxtimes} S_i^z = 0$: these two constraints minimize the first term on the right-hand side of both Eqs. (2) and (3). The $M_{\boxtimes} = 0$ constraint corresponds to the so-called ice rule for square ice, and therefore we will hereafter denote the states which satisfy it (and which satisfy $S_i^z = \pm S$) as ice-rule states; (2) second, one needs to choose, among the ice-rule states, those corresponding to a minimum of the second term in the right-hand side of Eqs. (2) and (3); this term is always antiferromagnetic by construction, so that it can be minimized by zero-magnetization vertices.

In the special case $J_1 = J_2$, we recover $\mathcal{H} = J_{1(2)}h_{\text{ice}}$, namely, the square-ice model, the ground states of which are only constrained by the ice rule (along with the condition $S_i^z = \pm S$). The ground-state properties of this system are equivalent to the six-vertex model, displaying an exponential degeneracy of the ground state.[13] This degeneracy is (partially) lifted when $J_1 \neq J_2$.

If $J_1 > J_2$, we need to select among all zero-magnetization vertices with satisfied antiferromagnetic J_1 bonds. This further constraint imposes that each vertex must take the antiferromagnetic (Néel) configuration in Fig. 2(b) or its spin-flipped version (two-vertex model), and it reduces the possible ground states to the two Néel-ordered states. The ground-state energy per spin takes the value $E_{\text{Néel}} = -(2J_1 - J_2)S^2$.

If, on the contrary, $J_2 > J_1$, the zero-magnetization vertices must satisfy the J_2 bonds, and therefore they take one of the four collinear configurations in Fig. 2(b), reducing the ground state of the system to that of a four-vertex model. The collinear ground states (namely, containing only collinear vertices) are massively degenerate because flipping a linear chain of spins along the J_2 diagonals does not alter any of the constraints which the ground state must satisfy. Therefore, the ground-state degeneracy is equal to 2^{N_d}, where N_d is the number of J_2 diagonals. The ground-state energy per spin takes the value $E_{\text{coll}} = -J_2 S^2$.
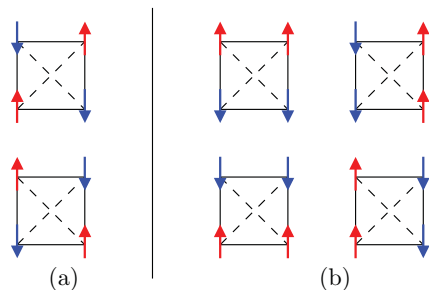
FIG. 2. (Color online) Crossed plaquettes that obey the "ice rule." (a) On the Néel plaquettes, the nearest-neighbor links are satisfied. (b) On the "collinear" plaquettes, the next-nearest-neighbor links are satisfied.

In summary, the degeneracy of the ice-rule states is partially lifted when $J_1 \neq J_2$, and ice-rule states are organized into a band with energy width (per spin) given by

$$\omega = |E_{\text{Néel}} - E_{\text{coll}}| = 2|J_1 - J_2|S^2. \tag{5}$$

The above discussion is valid for an arbitrary value of the spin length S, and in particular also in the classical limit $S \rightarrow \infty$, in which one can introduce continuous spins $\tilde{S}_i = S_i/S$ with unit length $|\tilde{S}_i|^2 = 1$. On the other hand, we will see that the application of a transverse field introduces significant differences for the ground-state properties depending on the spin length S.

B. Excited states in zero field

The nature of the excited states is dependent upon the spin length. In the following, we will concentrate on the $S = 1/2$ case, which will be the main focus of this paper. In this limit, when $J_1 > J_2$, the lowest-energy excitations correspond either to one of the following: (1) a single spin flip, costing an energy

$$\Delta = (2 - \nu_1)J_1 + (1 - \nu_2)J_2, \tag{6}$$

where ν_p is the number of frustrated J_p links ($p = 1, 2$) connected to each site. For Néel states, $\nu_1 = 0$ and $\nu_2 = 2$, while for collinear states $\nu_1 = 2$ and $\nu_2 = 0$. Notice that for generic ice-rule states, one has $\nu_1 + \nu_2 = 2$; (2) a joint flip of all the spins on a plaquette (plaquette flip). This operation has the lowest energy when applied to a *flippable* plaquette, with the property that its flip connects the initial ice-rule state to another ice-rule state. All the neighboring vertices of a flippable plaquette share with the plaquette a bond with zero magnetization, so that the plaquette flip will not alter the vertex magnetization. This imposes that the flippable plaquette has a local Néel configuration. In Néel states, all plaquettes are flippable, with an energy cost of $\Delta_{\text{plaq}} = 4(J_1 - J_2)$. In the collinear states, only a portion of the plaquettes are flippable (at most one half as in the state depicted in Fig. 3), with an energy cost of $\Delta_{\text{plaq}} = 4(J_2 - J_1)$.

Comparing the energy cost of a plaquette flip with that of a spin flip, we find that plaquette flips are the lowest-energy excitations in the parameter range $2/3 < J_2/J_1 < 4/3$, and outside of this range, spin flips are instead the excitations with the lowest energy.
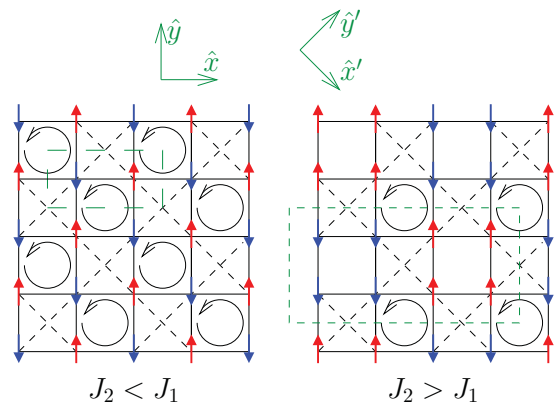

FIG. 3. (Color online) Reference classical ground states. The circles indicate flippable plaquettes.

C. $S \rightarrow \infty$ limit in a transverse magnetic field

In this section, we discuss the effect of a transverse field on classical continuous spins ($S \rightarrow \infty$). The corresponding ground-state configurations will serve as a template for the spin-wave analysis in the quantum case. The transverse field introduces a canting of the spins along the x axis by an angle ϑ (see Fig. 4). This angle increases with the intensity of the field up to a critical value Γ_c at which $\vartheta = \pi/2$, corresponding to the polarization of the spins along x. For both the collinear and the Néel ground states, each spin sees the same local field (in modulus) created by the neighboring spins [$\boldsymbol{h}_{\text{loc}} = \pm(4J_1 - 2J_2)S\hat{z}$ for Néel states, and $\boldsymbol{h}_{\text{loc}} = \pm 2J_2 S\hat{z}$ for collinear states, where $\hat{z}$ is the unit vector in the z direction of spin space]. Therefore, the application of the external field will create the same canting angle ϑ on each spin. Upon canting, the spin configuration becomes $S_i^x = S \sin \vartheta$ and $S_i^z = \pm S \cos \vartheta$.

The classical energy per spin admits the compact expression, valid for both the Néel and collinear states:

$$\varepsilon_{\text{cl}} = [(\nu_1 - 2)J_1 + (\nu_2 - 1)J_2]S^2 \cos^2 \vartheta - \Gamma S \sin \vartheta$$
$$= [\nu_2(J_2 - J_1) - J_2]S^2 \cos^2 \vartheta - \Gamma S \sin \vartheta. \tag{7}$$

Minimizing the energy per spin with respect to ϑ, we find

$$\sin \vartheta = \min\left(\frac{\Gamma}{2S[J_2 - \nu_2(J_2 - J_1)]}, 1\right). \tag{8}$$

If $\Gamma > \Gamma_c = 2S[J_2 - \nu_2(J_2 - J_1)]$, the system becomes completely polarized in the transverse direction. For $\Gamma > \Gamma_c$, the classical ground-state energy per spin takes the value

$$\varepsilon_{\text{cl}} = -S^2[J_2 - \nu_2(J_2 - J_1)](1 + \sin^2 \vartheta). \tag{9}$$

The resulting classical phase diagram for $S \rightarrow \infty$ is shown in Fig. 5.
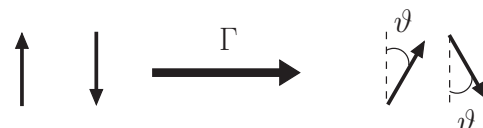

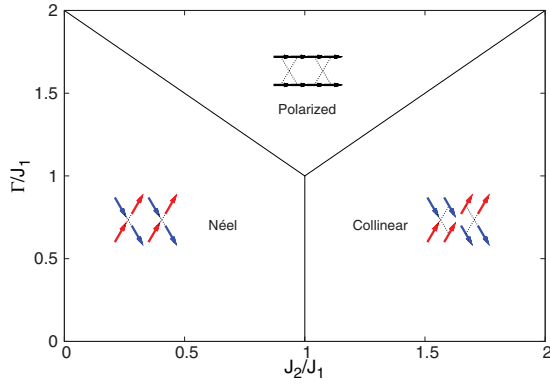FIG. 4. Classical rotation angle induced by the transverse field.

FIG. 5. (Color online) Classical phase diagram of the transverse-field Ising model on the checkerboard lattice.

III. SQUARE ICE IN A TRANSVERSE FIELD: RESULTS FROM PERTURBATION THEORY

For square ice ($J_1 = J_2$), in the case $\Gamma \ll J_1, J_2$, the transverse field can be treated via degenerate perturbation theory on the manifold of ice-rule states. Considering all terms up to fourth order,[26] one can easily find the following effective Hamiltonian for the subspace of ice-rule states (up to an additive constant):

$$\mathcal{H}_{\text{eff}} = -\frac{\Gamma^4}{\Delta^3} \sum_{\text{flippable}\square} (S_i^+ S_j^- S_k^+ S_l^- + \text{H.c.}) + \mathcal{O}\left(\frac{\Gamma^6}{\Delta^5}\right), \quad (10)$$

where ($ijkl$) are the four sites on a plaquette (in clockwise order), and the sum runs on flippable plaquettes. Various claims exist in the literature[11,14] that this Hamiltonian will lift the degeneracy of ice-rule states in favor of the Néel state, based on the fact that the Néel state has the largest number of flippable plaquettes. In fact, this Hamiltonian is completely off diagonal for the ice-rule states, so that it can not favor a specific ice-rule state, but only a resonant superposition thereof. In particular, a flippable plaquette, once flipped, turns its four neighboring vertices from Néel configurations to collinear configurations or vice versa, namely, the effective Hamiltonian will resonantly connect local Néel configurations with local collinear ones. At the same time, two corner-sharing flippable plaquettes can not be both flipped without leaving the ice-rule manifold, which suggests that Néel-collinear resonances will be localized to single plaquettes. A rough approximation to the ground state of Eq. (10) is therefore a state in which a checkerboard subset of non-corner-sharing plaquettes resonate between two flippable states, giving rise to a resonating-plaquette solid (RPS)

$$|\Psi_0\rangle \approx |\Psi_{\text{RPS}}\rangle = \prod_{\square}{}' (|\uparrow_i \downarrow_j \uparrow_k \downarrow_l\rangle + |\downarrow_i \uparrow_j \downarrow_k \uparrow_l\rangle)/\sqrt{2}, \quad (11)$$

where the primed product runs on a sublattice of plaquettes. This state breaks the twofold symmetry between the two plaquette sublattices. While direct numerical investigations of the square-ice model in a transverse field are not known to us, there exists in the literature a series of numerical studies of square ice with different quantum perturbations, which all map perturbatively onto the effective Hamiltonian of Eq. (10). A direct simulation of Eq. (10) is reported in

Ref. 15, while Refs. 16, 17, and 18 focus on hard-core bosons on the checkerboard lattice at half-filling, with strong nearest-neighbor repulsion, and weak hopping (with either positive or negative sign) between nearest neighbors and next-to-nearest neighbors. The latter model is equivalent to square ice with weak ferromagnetic/antiferromagnetic exchange terms for the x and y spin components. The common result of all these studies is that the ground state for weak quantum perturbations has indeed long-range RPS order, and no magnetic order. Therefore, we expect spin-wave theory to break down or become inconclusive in this limit, which is indeed one of the main results of the following analysis.

IV. LINEAR SPIN-WAVE THEORY

In the following, we describe a treatment of quantum fluctuations introduced by the transverse field in the $S = 1/2$ case based on a linear spin-wave expansion.[25,27] We will then treat separately the spectrum of excitations above the various classical reference states of the system: Néel, collinear, and fully polarized.

A. Spin-boson transformation

We begin by considering a generic classical ground state with long-range magnetic order, and with a magnetic unit cell containing n spins. We denote $S_{l,p}$ the pth spin ($p = 1 \ldots n$) of the lth cell. As seen in Sec. II C, in the classical limit an applied transverse field introduces a canting of the spins by an angle ϑ with respect to the z axis. We introduce a local rotation of the spin configuration $\tilde{S}_{l,p} = \sigma_p \mathcal{R}_y(\sigma_p \vartheta) S_{l,p}$, where $\sigma_p = 1 \, (-1)$ if the spin in zero field has positive (negative) projection along the z axis, and $\mathcal{R}_y(\pm \vartheta)$ is the rotation matrix of an angle $\pm \vartheta$ around the y axis. In the classical limit $S \to \infty$, the ground state is a simple ferromagnetic state for the $\tilde{S}_{l,p}$ spins, namely, $\tilde{S}_{l,p}^z = S$ everywhere.

We then consider small quantum fluctuations around this classical reference state by transforming the quantum spins to bosons via a linearized Holstein-Primakoff transformation[28] valid in the limit of a small number of bosons $n_{l,p} \ll 2S$:

$$\tilde{S}_{l,p}^z = S - a_{l,p}^\dagger a_{l,p} \quad \tilde{S}_{l,p}^x \approx \sqrt{\frac{S}{2}}(a_{l,p}^\dagger + a_{l,p}). \quad (12)$$

Here, $a_{l,p}$ and $a_{l,p}^\dagger$ are bosonic operators, satisfying $[a_{l,p}, a_{l,p}^\dagger] = 1$ and $[a_{l,p}^{(\dagger)}, a_{l,p}^{(\dagger)}] = 0$.

B. Harmonic Hamiltonian for ordered ice-rule states

The Hamiltonian is then expanded up to quadratic order in the bosonic operators (the linear terms vanish by construction). In the following, we will specialize the discussion to reference classical states which in zero field are ice-rule states with long-range magnetic order, namely, the states which minimize the energy in the classical limit $S \to \infty$, and the ordered structure of which allows us to build a spin-wave theory. These states have the property that the number of frustrated bonds of types 1 and 2, ν_1 and ν_2, is the same for every site. Under these generic assumptions, the quadratic bosonic Hamiltonian reads

as

$$\mathcal{H}_{\text{LSW}} = N\varepsilon_{\text{cl}} + J_1\tilde{\mathcal{H}}_{nn} + J_2\tilde{\mathcal{H}}_{nnn} + \Gamma\tilde{\mathcal{H}}_\Gamma \qquad (13)$$

with

$$\tilde{\mathcal{H}}_{nn} = 2S\nu_2\cos^2\vartheta\sum_{l,p}a_{l,p}^\dagger a_{l,p} + \frac{S}{2}\sin^2\vartheta$$

$$\times \sum_{\langle lp,l'p'\rangle}(a_{l,p}^\dagger a_{l',p'}^\dagger + a_{l,p}^\dagger a_{l',p'} + \text{H.c.}),$$

$$\tilde{\mathcal{H}}_{nnn} = 2S(1-\nu_2)\cos^2\vartheta\sum_{l,p}a_{l,p}^\dagger a_{l,p} + \frac{S}{2}\sin^2\vartheta \qquad (14)$$

$$\times \sum_{\langle\langle lp,l'p'\rangle\rangle}(a_{l,p}^\dagger a_{l',p'}^\dagger + a_{l,p}^\dagger a_{l',p'} + \text{H.c.}),$$

$$\tilde{\mathcal{H}}_\Gamma = -\Gamma\sin\vartheta\sum_{l,p}a_{l,p}^\dagger a_{l,p}.$$

This is a remarkable result in that the spin-wave Hamiltonian depends only on the frustration parameters ν_1 and ν_2, while it is completely independent of the geometry of the unit cell. The frustration parameters ν_1, ν_2 distinguish among Néel states and collinear states, but they are *not* able to distinguish among different collinear states. At the square-ice point $J_1 = J_2$, the dependence on the frustration parameter drops. Therefore, as we will discuss further, quantum corrections at the harmonic level are not able to lift the degeneracy between ordered ice-rule states, regardless of the size of their magnetic unit cell. This result can be extended even to disordered ice-rule states, which can be regarded as ordered ones with an infinite unit cell.

To diagonalize the spin-wave Hamiltonian, Eq. (14), we first introduce the Fourier transform of the bosonic operators and then perform a n-modes Bogoliubov transformation as described in Appendix A. The Hamiltonian then becomes

$$\mathcal{H} = N\left(\varepsilon_{\text{cl}} - \frac{\varepsilon_0}{2}\right) + \frac{1}{2}\sum_{\mathbf{k},p}\omega_{\mathbf{k},p}\left(b_{\mathbf{k},p}^\dagger b_{\mathbf{k},p} + \frac{1}{2}\right), \qquad (15)$$

where $\varepsilon_0 = 2S[J_2 - \nu_2(J_2 - J_1)]$.

C. Néel state

Let us first consider the Néel state, defined for $\Gamma < 2S(2J_1 - J_2)$. Its unit cell contains $n = 2$ spins (see Fig. 3). The unit cells form a rotated square lattice with vectors $\hat{x}' = (\hat{x} - \hat{y})$ and $\hat{y}' = (\hat{x} + \hat{y})$. The diagonalization of the Hamiltonian shows that the spectrum of the magnon excitations is gapped whenever the classical Néel state is defined, i.e., if $\Gamma < 2S(2J_1 - J_2)$ (details are given in Appendix A). Its lower band is plotted in Fig. 6. It has minima at $(0,0)$ and at the four corners of the Brillouin zone. This corresponds to the structure of the classical Néel state.

D. Collinear states

As already mentioned in Sec. IV A, all collinear states admit the same frustration parameter ν_2, and hence the same spin-wave Hamiltonian. This means that they possess the same spectrum of harmonic spin-wave excitations (but folded into a smaller Brillouin zone, the larger the unit cell), and that
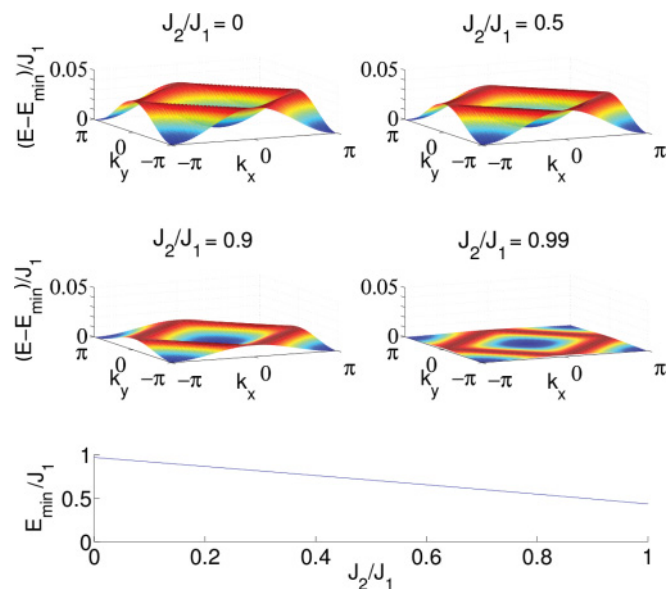

FIG. 6. (Color online) Lowest band of the magnon spectrum for $\Gamma = J_1/2$ and various values of J_2/J_1, around the Néel state. For the purpose of readability, the bands have been offset by the energy of their lower edge. The lower band edge (corresponding to the minimum excitation gap) is plotted in the lower panel.

zero-point quantum fluctuations can not lift the degeneracy among them.

We will then specify the discussion to the particular collinear state represented in Fig. 3. Its unit cell contains $n = 8$ spins; the unit cells form a square lattice with vectors $\hat{x}' = 2(\hat{x} - \hat{y})$ and $\hat{y}' = 2(\hat{x} + \hat{y})$. While not being the simplest of all collinear states, this state is relevant because it can be energetically stabilized against other collinear states by, e.g., dipolar interactions, which are relevant for realistic ice models.[29] The magnon dispersion relation, obtained by diagonalizing $M_\mathbf{k}$, is shown in Fig. 7. It shows a finite gap, and two *lines* of minimum-energy degenerate modes along the axes of the first Brillouin zone of the magnetic lattice (1/8 of the Brillouin zone of the geometric lattice, shown in Fig. 7). These degenerate modes traveling with momentum $(k_x, \pm k_x)$ for all k_x values can be associated with deconfined monopolelike[30] pairs, obtained by flipping a finite string of spins along a J_2 diagonal of the checkerboard lattice. Given the degeneracy of all collinear states, not perturbed by quantum fluctuations, these pairs are deconfined along the J_2 diagonals, and their energy is independent of momentum as long as it satisfies the constraint of diagonal motion.

E. Quantum square ice

At the square-ice point $J_1 = J_2 = J$, spin-wave theory built around any ice-rule state with canting spins produces the same excitation spectrum and zero-point quantum fluctuations. Therefore, harmonic quantum fluctuations are not able to lift the degeneracy of the classical ice-rule manifold, and the elementary excitations are identical to the classical case, namely, deconfined monopole pairs moving with arbitrary momentum. This is reflected in the spin-wave dispersion, showing a *perfectly flat* band for the lowest-energy excitations,
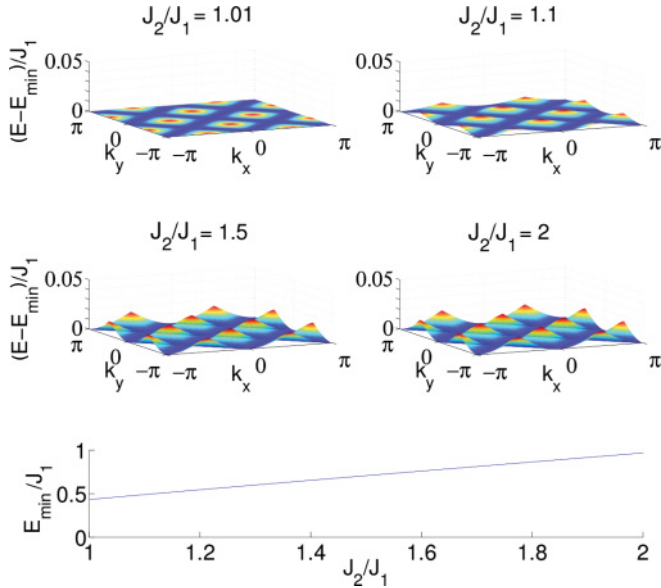
FIG. 7. (Color online) Lowest band of the magnon spectrum for $\Gamma = J_1/2$ and various values of J_2/J_1, around any collinear state. For the purpose of readability, the bands have been offset by the energy of their lower edge. The lower band edge (corresponding to the minimum excitation gap) is plotted in the lower panel.
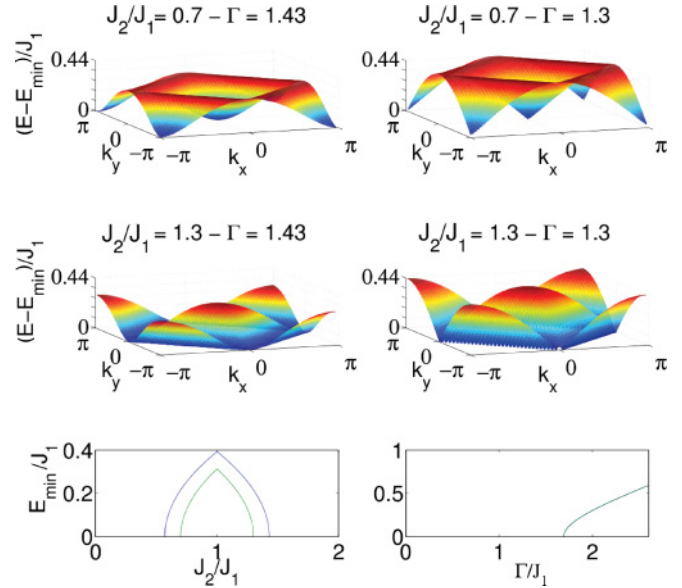

FIG. 8. (Color online) Upper panels: lowest band of the magnon spectrum around the polarized state for $\Gamma > \Gamma_c$ (left column) and for $\Gamma = \Gamma_c$ (right column). Lower panels: Minimum excitation gap: (left) as a function of J_2/J_1 for $\Gamma/J_1 = 1.3$ (green line) and for $\Gamma/J_1 = 1.43$ (blue line); (right) as a function of Γ/J_1 for $J_2/J_1 = 0.7$ and 1.3 (the curves for both cases coincide).

and with a gap equal to the classical value, namely, $\Delta_{\text{cl}} = 2\varepsilon_0 = 2JS^2$.

F. Polarized states

For large Γ, the classical reference state is totally polarized along the field. Nonetheless, quantum fluctuations introduce deviations from the polarized state, given that the field term in the Hamiltonian does not commute with the Ising couplings. We build a spin-wave Hamiltonian around the polarized state analogously to what has been done for the ice-rule states. Even though in the classical spin configuration all the spins have the same orientation, the magnetic unit cell contains two sites (exactly as in the case of the Néel state), due to the fact that the checkerboard lattice is not a Bravais lattice. The bosonic excitations correspond to deviations of the spin from full polarization along the x axis.

The magnon spectrum is shown in Fig. 8. It displays softer modes at the four corners of the square-lattice Brillouin zone (for $J_1 > J_2$), and along the edges of the checkerboard-lattice Brillouin zone (for $J_1 < J_2$). These modes become gapless when approaching the critical field Γ_c, signaling the instability of the fully polarized state to a Néel state (for $J_1 > J_2$) and to degenerate collinear states (for $J_1 < J_2$).

V. RESULTS OF THE SPIN-WAVE ANALYSIS

The main observables from linear spin-wave theory are represented by the internal energy $E = \langle \mathcal{H}_{\text{LSW}} \rangle$ and the order parameter $m = \langle \tilde{S}^z \rangle / S$, the expressions of which are given in Appendix B. These two quantities allow us to extract the quantum phase diagram of our system in the harmonic approximation.

For each value of J_2 and Γ, we can *a priori* choose between three families of reference states as candidate ground state:

the Néel states, the fully polarized state, and the degenerate collinear states. Notice that classically, the Néel and the collinear states differ in the value of the correlations between next-to-nearest neighbors $C^{(2)} = \langle S_i^z S_j^z \rangle_{\langle\langle i,j \rangle\rangle} = (\nu_2 - 1)$. For the Néel state, $C_{\text{Néel}}^{(2)} = S^2$, whereas for all collinear states, $C_{\text{collinear}}^{(2)} = -S^2$. A natural definition of the ground state (or ground-state manifold) identified by spin-wave theory is the state (or the family of states) which has the lowest energy, the order parameter of which is finite and the next-to-nearest-neighbor correlations of which have the correct sign; moreover, the stability of the state requires also that the spin-wave frequencies be real numbers. The satisfaction of these four conditions allows us to identify the phases indicated in Figs. 9 and 10, which correspond to the classical phases for the same parameter ranges.

A clear region of instability of spin-wave theory is found close to the classical transition line between the fully polarized phase and the Néel and collinear phases, as indicated by the black region in Fig. 10. In this parameter range, the order parameters for *all* reference states are found to vanish, as shown in Fig. 11, clearly signaling the onset of a quantum-disordered phase.

However, a number of other anomalies revealed by the linear spin-wave theory close to the transition to the paramagnetic phase point to a significantly larger region where the classical behavior is probably destroyed by quantum fluctuations.

First of all, a qualitative deviation from the classical behavior is observed when approaching the square-ice limit $J_1 = J_2$ in a strong field $0.7 \lesssim \Gamma \lesssim J_1$. In this range (indicated by the dense-hatched region in Fig. 9), we observe an inversion of the energy hierarchy between Néel and collinear states with respect to the classical case. This occurs despite the fact
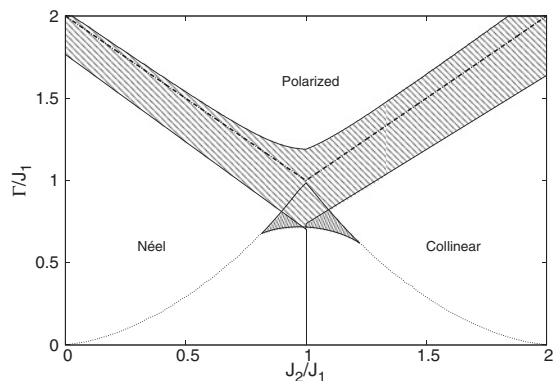
FIG. 9. Phase diagram of the $S = 1/2$ transverse-field Ising model on a checkerboard lattice from spin-wave theory. The hatched and dense-hatched regions correspond to the next-to-nearest neighbor correlation inversion region and to the energy-hierarchy inversion region, respectively (see text). Below the dotted lines, one can find, in the classical limit, two states which are (local) energy minima and which have order in the z-spin components: one state with Néel order, and the other with collinear order. Above this line, one of the two states becomes the polarized state. Therefore, collinear and Néel ordered states can only be compared energetically below the dotted line.

that quantum fluctuations are stronger for the energetically favored phase, as shown by the order parameters of the two phases obeying an opposite hierarchy (namely, $m_{\text{Néel}} > m_{\text{collinear}}$ when $E_{\text{Néel}} > E_{\text{collinear}}$, and vice versa, see Fig. 12). The inversion in the energy hierarchy is due to strong quantum corrections to the classical energy, which change qualitatively the dependence of both Néel and collinear energies on J_2/J_1.

This strong quantum effect of energy hierarchy inversion suggests that classical order might be unstable around the hierarchy inversion region in Fig. 9 when considering quantum fluctuations beyond linear spin-wave theory. The real ground state of the system may then be an intermediate phase which can not be described within the linear spin-wave approximation.

Another strong quantum effect is revealed close to the classical phase boundaries. While classically $E_{\text{Néel}}$ and $E_{\text{collinear}}$ are monotonic functions of J_2/J_1, they become nonmonotonic around the above-mentioned field range. In particular, $E_{\text{Néel}}$
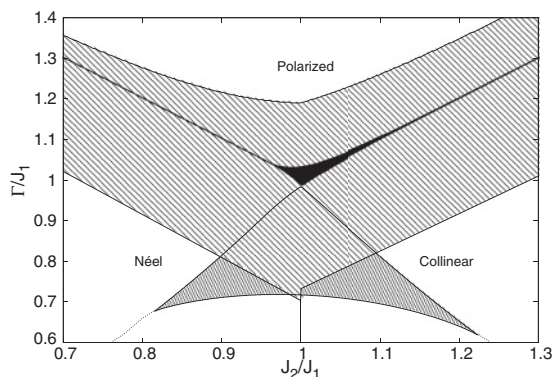

FIG. 10. Zoom of Fig. 9 around the classical tricritical point. In the black domain, the order parameters of all considered phases vanish. Other marked zones are as in Fig. 9.
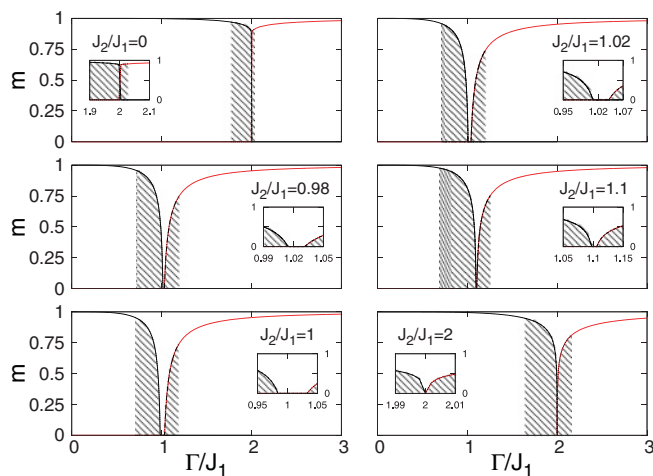

FIG. 11. (Color online) Order parameter vs field for different values of J_2. It vanishes at the critical value of the field and a small gap opens for J_2 close to J_1 where none of the three states has a finite order parameter. The insets are closer views around the critical value of the field. The hatched and dense-hatched regions correspond to those identified in the phase diagram (Fig. 9).

grows with increasing J_2/J_1 until it reaches a maximum, beyond which it starts to decrease; from a classical point of view, this is quite surprising. According to the Hellmann-Feynman theorem, the next-nearest-neighbor correlations $C^{(2)}$ are given by the derivative of the energy with respect to J_2, namely, $C^{(2)} = \partial \langle \mathcal{H} \rangle / \partial J_2$. Consequently, a change of sign in the derivative of E corresponds to a change of sign in $C^{(2)}$, which means that the harmonic ground state is dramatically different from the reference state. The locus of the maxima in the energy as a function of J_2/J_1 represents the lower bound of the hatched region in Figs. 9 and 10.

A further element of inconsistency of spin-wave theory is offered by the apparent violation of the Hellman-Feynman theorem

$$\langle S_x \rangle = -\frac{\partial \langle \mathcal{H} \rangle}{\partial \Gamma}. \qquad (16)$$
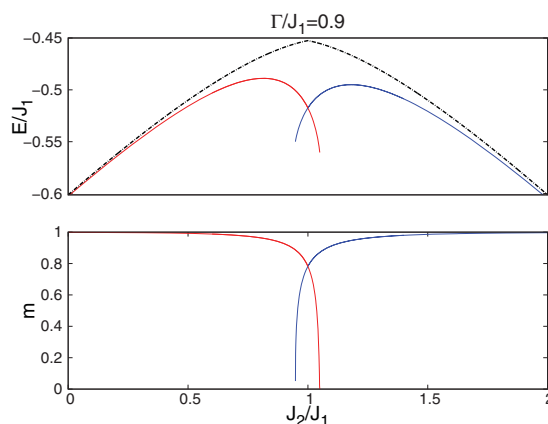

FIG. 12. (Color online) Average energy (upper panel) and order parameter (lower panel) associated with the Néel (red solid line) and collinear (blue solid line) reference states. The dashed lines correspond to the classical energies. Both panels are for $\Gamma/J_1 = 0.9$.
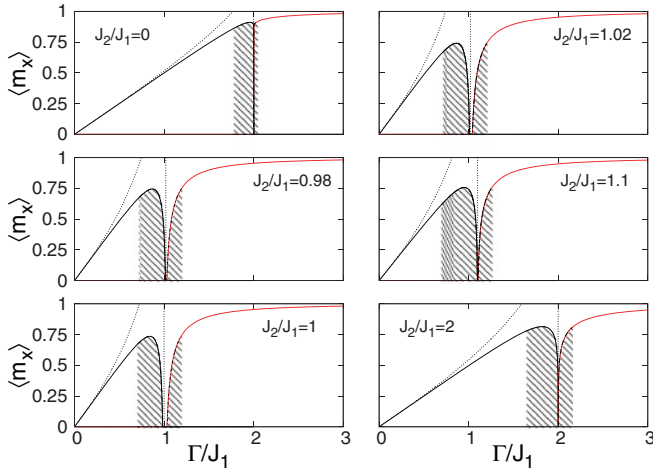
FIG. 13. (Color online) Field-induced magnetization as a function of the field for different values of J_2/J_1. The highlighted regions are as in Fig. 11. The dotted lines correspond to the opposite of the derivatives of the average energies with respect to the magnetic field Γ. These curves deviate from the average induced magnetization, signaling a violation of the Hellmann-Feynman theorem (see text).

The transverse magnetization, defined as $\langle m_x \rangle = \langle S^x \rangle$, is proportional to m in the harmonic approximation: $\langle S_x \rangle = S \sin \vartheta \, m$. The deviation from Eq. (16) comes along with a strong nonmonotonic behavior, as shown in Fig. 13. This behavior is unphysical, implying a negative susceptibility. This signals again that an ordered reference state does not lead to consistent results. We identify therefore an additional region of strong anharmonic fluctuations with the magnetization dip in the m_x versus Γ curve. This dip lies inside the region $[\Gamma_1, \Gamma_2]$ where $\frac{\partial m_x}{\partial \Gamma}(\Gamma_1) = 0$ and $m_x(\Gamma_2) = m_x(\Gamma_1)$. The latter condition marks the upper bound of the hatched region in Figs. 9 and 10.

Indeed, Eq. (16) ceases to be strictly valid in the linear spin-wave approximation because in general the linear spin-wave Hamiltonian does *not* have the form $\mathcal{H} = \mathcal{H}_0 - \Gamma S^x$. From inspection of Eqs. (13) and (14), it is immediate to see that each term of the Hamiltonian depends on Γ through $\theta(\Gamma)$, except for the polarized case in which $\theta = \pi/2$ independently of the value of Γ. In fact, to recover the identity of Eq. (16) at order $1/S$, one has to include corrections to the harmonic ground state.[31] Even though Eq. (16) ceases to be an identity within linear spin-wave theory, the precision with which Eq. (16) is approximately verified can be used as a further criterion for the validity of the linear spin-wave approximation. In Fig 13, $\langle S_x \rangle$ is compared to $\partial \langle \mathcal{H} \rangle / \partial \Gamma$: upon increasing the field, the quantities show a significant deviation from each other when approaching the region already identified before as showing significant inconsistencies of spin-wave theory.

A strong violation of the Hellman-Feynman theorem Eq. (16) is observed also in the case $J_2 = 0$. In this limit, the system reduces to the square-lattice Ising model in a transverse field, which features a well-known quantum phase transition [for a field $\Gamma_c/J_1 \approx 1.5$ (see Ref. 32)] between Néel order and a quantum paramagnetic state. Interestingly, the deviation

between m_x and $\partial \langle \mathcal{H} \rangle / \partial \Gamma$ builds up when approaching the quantum-critical field Γ_c, showing that spin-wave theory is able to signal the quantum phase transition via the breakdown of the consistency of its results with known theorems.

VI. CONCLUSIONS AND DISCUSSION

In this study, we have applied a linear spin-wave-theory analysis to the transverse-field Ising model on the checkerboard lattice, which represents a paradigmatic example of a frustrated Ising model with controlled quantum fluctuations. We find the remarkable result that harmonic quantum fluctuations are not able to lift the classical degeneracy, which is exponential in the linear dimension of the system when the next-to-nearest-neighbor coupling J_2 exceeds the nearest-neighbor one J_1, and which is exponential in the system size for $J_1 = J_2$, corresponding to the square-ice limit. This implies that spin-wave theory is inconclusive regarding the question of which classical ground state is selected by quantum effects, and that nonlinear quantum fluctuations play a central role in lifting the degeneracy in the exact ground state. This result is consistent with existing studies of the square ice in a weak transverse field, for which degenerate perturbation theory and numerics suggest a quantum-disordered ground state with the structure of a resonating plaquette solid.

Our results suggest that a quantum-disordered ground state persists beyond this limit. Spin-wave theory indicates an anomalous inversion in the classical hierarchy between reference states for strong fields and for $J_1 \sim J_2$, suggesting that quantum fluctuations beyond the harmonic approximation can destroy classical order in the system in that parameter range. Moreover, spin-wave theory breaks down completely close to the classical transition line to full polarization, where linear quantum fluctuations are able to suppress all spin components. This identifies an interesting candidate region for quantum-disordered ground states.

Recent experimental developments have led to controlled realizations of frustrated Ising models, both in the classical limit and in the presence of tunable transverse fields. In particular, the classical square-ice model, enriched with long-range dipolar interactions, is realized in recent experiments on square-lattice arrays of nanopatterned magnetic domains.[33] While quantum tunneling of the magnetization in these systems is not realistic, given the mesoscopic size of the magnetic moments, one can envisage scaling down the components of these artificial ice systems to single-molecule magnets,[34] which can be arranged into regular arrays on a surface.[35] Transverse-field Ising models are currently realized by arrays of trapped ions,[36–38] where the internal states of the ions can be coupled with Ising Hamiltonians via virtual phonons, and where transverse fields are created by Raman laser schemes. The ions can be individually trapped by microtraps, which can in turn be arranged into arbitrary planar arrays,[39] encompassing the checkerboard geometry explored here as well as other frustrated structures. Therefore, the theoretical investigation of transverse-field Ising models on frustrated lattices is very compelling, as it promises to lead to the realization of novel quantum states in controlled artificial spin systems in the near future.

APPENDIX A: SPIN-WAVE THEORY FOR GENERAL ISING HAMILTONIANS IN A TRANSVERSE FIELD

We present here several general formulas to study the quadratic quantum fluctuation in a generic transverse field Ising system. We consider a generic classical ground state with long-range magnetic order, and with a magnetic unit cell containing n spins. We denote $S_{l,p}$ the pth spin ($p = 1 \ldots n$) of the lth cell. The most general Hamiltonian supporting such a ground state has the form

$$\mathcal{H}_{\mathrm{TFI}} = \frac{1}{2} \sum_{lp,l'p'} [J(\boldsymbol{r}_{l'} - \boldsymbol{r}_l)]_{pp'} S_{l,p}^z S_{l',p'}^z - \Gamma \sum_i S_{l,p}^x. \quad (A1)$$

Here, $\boldsymbol{r}_l$ is the position of a reference site in the lth unit cell, and $J(\Delta \boldsymbol{r})$ is a $n \times n$ matrix containing the couplings between spins in unit cells at a distance $\Delta \boldsymbol{r}$.

In the classical limit, an applied transverse field rotates the pth spins around the y axis by an angle ϑ_p. As already discussed in Sec. IV A, we introduce a local rotation of the spin configuration $\tilde{S}_{l,p} = \sigma_p \mathcal{R}_y(\sigma_p \vartheta_p) S_{l,p}$, where $\sigma_p = \pm 1$ is the orientation of the spin in zero field. The rotation has the effect of reducing the $S = \infty$ ground state to a perfectly ferromagnetic one. The classical energy of the pth spin of each cell has the expression

$$\varepsilon_{\mathrm{cl},p} = \frac{S^2}{2} \sigma_p \cos \vartheta_p \sum_{\Delta \boldsymbol{r}, p'} [J(\Delta \boldsymbol{r})]_{pp'} \sigma_{p'} \cos \vartheta_{p'} - S\Gamma \sin \vartheta_p,$$

so that the total classical energy can be written as

$$E_{\mathrm{cl}} = \frac{N}{n} \sum_p \varepsilon_{\mathrm{cl},p} = \frac{N}{n} \mathrm{Tr} \, \varepsilon_{\mathrm{cl}}, \quad (A2)$$

where we have introduced the matrix $[\varepsilon_{\mathrm{cl}}]_{p,p'} = \varepsilon_{\mathrm{cl},p} \delta_{p,p'}$.

We then consider small quantum fluctuations around this classical reference state by transforming the quantum spins to bosons via a linearized Holstein-Primakoff transformation[28] valid in the limit of a small number of bosons $n_{l,p} \ll 2S$:

$$\tilde{S}_{l,p}^z = S - a_{l,p}^\dagger a_{l,p} \quad \tilde{S}_{l,p}^x \approx \sqrt{\frac{S}{2}} (a_{l,p}^\dagger + a_{l,p}). \quad (A3)$$

Here, $a_{l,p}$ and $a_{l,p}^\dagger$ are bosonic operators, satisfying $[a_{l,p}, a_{l,p}^\dagger] = 1$ and $[a_{l,p}^{(\dagger)}, a_{l,p}^{(\dagger)}] = 0$. The angles ϑ_p are chosen so that the classical reference state is stable. Thus, the linear terms in the bosonic operators vanish.

The quadratic Hamiltonian then reads as

$$8\mathcal{H}_2 = E_{\mathrm{cl}} + \sum_{l,p} \tilde{h}_p a_{lp}^\dagger a_{lp}$$

$$+ \frac{1}{2} \sum_{lp,l'p'} \tilde{J}(\boldsymbol{r}_{l'} - \boldsymbol{r}_l)_{pp'} (a_{lp}^\dagger + a_{lp})(a_{l'p'}^\dagger + a_{l'p'}),$$

$$(A4)$$

where

$$\tilde{h}_p = 2\varepsilon_{\mathrm{cl},p}/S + \Gamma \sin \vartheta_p,$$

$$\tilde{J}(\Delta \boldsymbol{r})_{pp'} = J(\Delta \boldsymbol{r})_{pp'} \sin \vartheta_p \sin \vartheta_{p'}. \quad (A5)$$

We then introduce the Fourier transform of the bosonic operators and of the interaction

$$a_{\mathbf{k},p} = \sqrt{\frac{2}{N}} \sum_l e^{i\mathbf{k}\cdot\boldsymbol{r}_l} a_{l,p},$$

$$J(\mathbf{k}) = \sum_l e^{-i\mathbf{k}\cdot\Delta\boldsymbol{r}} \tilde{J}(\Delta\boldsymbol{r}). \quad (A6)$$

The quadratic Hamiltonian can then be written in the compact form

$$\mathcal{H}_2 = \frac{N}{n} \sum_p \left(\varepsilon_{\mathrm{cl},p} - \frac{\tilde{h}_p}{2} \right) + \frac{1}{2} \sum_{\mathbf{k}} A_{\mathbf{k}}^\dagger M_{\mathbf{k}} A_{\mathbf{k}}, \quad (A7)$$

where

$$\tilde{h}_p = \frac{2}{S} \varepsilon_{\mathrm{cl},p} + \Gamma \sin \vartheta_p,$$

$$A_{\mathbf{k}}^\dagger = (a_{\mathbf{k},1}^\dagger, \ldots, a_{\mathbf{k},n}^\dagger, a_{-\mathbf{k},1}, \ldots, a_{-\mathbf{k},n}),$$

$$M_{\mathbf{k}} = \begin{pmatrix} \Delta_{\mathbf{k}} & \Delta_{\mathbf{k}} \\ \Delta_{\mathbf{k}} & \Delta_{\mathbf{k}} \end{pmatrix} - \begin{pmatrix} \varepsilon_{\mathrm{cl}} & 0_n \\ 0_n & \varepsilon_{\mathrm{cl}} \end{pmatrix}, \quad (A8)$$

$$\Delta_{\mathbf{k}} = \frac{1}{2}(\tilde{J}(\mathbf{k}) + \tilde{J}(\mathbf{k})^\dagger).$$

This Hamiltonian can be diagonalized by a n-mode Bogoliubov transformation. This consists in finding the transformation $A_{\mathbf{k}} = T_{\mathbf{k}} B_{\mathbf{k}}$, with $B_{\mathbf{k}} = (b_{\mathbf{k},1}^\dagger, \ldots, b_{\mathbf{k},n}^\dagger, b_{-\mathbf{k},1}, \ldots, b_{-\mathbf{k},n})^T$, such that $A_{\mathbf{k}}^\dagger M_{\mathbf{k}} A_{\mathbf{k}} = \sum_p \omega_{\mathbf{k}}^{(p)} b_{\mathbf{k},p}^\dagger b_{\mathbf{k},p}$ and $[b_{\mathbf{k},p}, b_{\mathbf{k},p}^\dagger] = 1$ and $[b_{\mathbf{k},p}^{(\dagger)}, b_{\mathbf{k},p}^{(\dagger)}] = 0$.

We introduce the matrix Σ, given by

$$\Sigma = \begin{pmatrix} I_n & 0_n \\ 0_n & -I_n \end{pmatrix},$$

the matrix $Z_{\mathbf{k}}$ of the right eigenvectors of $\Sigma M_{\mathbf{k}}$, and the unitary matrix $U_{\mathbf{k}}$ such that $U_{\mathbf{k}}^\dagger Z_{\mathbf{k}}^\dagger \Sigma Z_{\mathbf{k}} U_{\mathbf{k}} = \mathrm{diag}(l_{\mathbf{k}}^{(1)}, \ldots, l_{\mathbf{k}}^{(n)}) = L_{\mathbf{k}}$. The transformation matrix $T_{\mathbf{k}}$ is then obtained as[40–42]

$$T_{\mathbf{k}} = Z_{\mathbf{k}} U_{\mathbf{k}} |L_{\mathbf{k}}|^{-1/2}. \quad (A9)$$

In particular, the eigenmodes $\omega_{\mathbf{k}}^{(p)}$ are the eigenvalues of $\Sigma M_{\mathbf{k}}$.

If the matrices $\Delta_{\mathbf{k}}$ and $\varepsilon_{\mathrm{cl}}$ commute (which is the case for the Néel and collinear states of the checkerboard Ising model studied here, having $\varepsilon_{\mathrm{cl}} = \varepsilon_0 I_n$), the eigenmodes $\omega_{\mathbf{k}}^{(p)}$ can be expressed in terms of the eigenvalues $\lambda_{\mathbf{k}}^{(p)}$ of $\Delta_{\mathbf{k}}$ in the form

$$\omega_{\mathbf{k}}^{(p)} = \frac{\varepsilon_{\mathrm{cl},p}}{2} \sqrt{1 + 4\frac{\lambda_{\mathbf{k}}^{(p)}}{\varepsilon_{\mathrm{cl},p}}}. \quad (A10)$$

APPENDIX B: ENERGY AND MAGNETIZATION IN THE CASE OF NÉEL AND COLLINEAR STATES

As mentioned above, in the particular case of the Néel and collinear states of the checkerboard-lattice Ising model studied in this work, the classical energies $\varepsilon_{\mathrm{cl},p}$ are all equal to ε_0. The

mean energy of the system then reads as

$$\langle E \rangle = N(\varepsilon_{cl} - \varepsilon_0/2) + \frac{1}{2}\sum_{\mathbf{k},p}\omega_{\mathbf{k},p}$$

$$= N\varepsilon_{cl} + \frac{\varepsilon_0}{4}\sum_{\mathbf{k},p}\left(\sqrt{1 + 4\frac{\lambda_{\mathbf{k},p}}{\varepsilon_0}} - 1\right). \quad (B1)$$

As $\Delta_{\mathbf{k}}$ is proportional to Γ^2, so are its eigenvalues. We can then expand the mean energy per spin in powers of Γ^2. We will introduce rescaled eigenvalues $\tilde{\lambda}_{\mathbf{k},p}$ defined as $\lambda_{\mathbf{k},p} = \varepsilon_0\Gamma^2\tilde{\lambda}_{\mathbf{k},p}$:

$$\langle \varepsilon \rangle = \varepsilon_{cl} + \frac{\varepsilon_0}{N}\sum_{\mathbf{k}}\sum_{m=1}^{\infty}\alpha_m\tilde{\lambda}_{\mathbf{k},p}^m\Gamma^{2m}$$

$$= \varepsilon_{cl} + \frac{\varepsilon_0}{N}\sum_{\mathbf{k},m}\alpha_m\mathrm{Tr}\left(\frac{\Delta_{\mathbf{k}}}{\varepsilon_0}\right)^m, \quad (B2)$$

where the α_m are defined by $\sqrt{1+4x} - 1 = 4\sum_{m=1}^{\infty}\alpha_m x^m$. In the case of a Néel or a collinear case, the trace of $\Delta_{\mathbf{k}}$ averages to zero in the Brillouin zone. Thus, the first nonzero correction to the classical energy in Eq. (B2) is of fourth order in Γ.

In both cases, if we introduce the ratio $J = J_2/J_1$, we get

$$\langle \varepsilon \rangle = \varepsilon_{cl} + \sum_{p>1}c_p(J)\left(\frac{J_1}{S(\nu_2 - J)^2}\right)^p\Gamma^{2p}, \quad (B3)$$

where the c_p coefficients only depend on J, and not on the considered state. It is then obvious that the expansion becomes independent of the classical state if $J = 1$. Thus, the classical degeneracy of the ice model is not lifted by harmonic fluctuations.

Similarly, if all the $\omega_{\mathbf{k},p}$ are real (which is the case whenever spin-wave theory holds), we have

$$m = 1 - \frac{1}{NS}\sum_{\mathbf{k},p}\langle a_{\mathbf{k}}^{\dagger(p)}a_{\mathbf{k}}^{(p)}\rangle$$

$$= 1 - \frac{1}{4NS}\sum_{\mathbf{k},p}\left(\frac{2\omega_{\mathbf{k},p}}{\varepsilon_0} + \frac{\varepsilon_0}{2\omega_{\mathbf{k},p}} - 2\right)$$

$$= 1 - \frac{1}{NS}\sum_{m=1}^{\infty}\sum_{\mathbf{k},p}\beta_m\widetilde{\lambda}_{\mathbf{k},p}^m\Gamma^{2m}, \quad (B4)$$

where the β_m are defined by $\sqrt{1+4x} + \frac{1}{\sqrt{1+4x}} - 2 = 4\sum_{m=1}^{\infty}\beta_m x^m$.

---

[1] *Introduction to Frustrated Magnetism: Materials, Experiments, Theory*, edited by C. Lacroix, F. Mila, and P. Mendels (Springer, Berlin, 2011).

[2] L. Balents, Nature (London) **464**, 199 (2010).

[3] Nonetheless, a spin-liquid ground state has been recently reported for the kagome lattice Heisenberg antiferromagnet, see S. Yan, D. A. Huse, and S. R. White, Science **332**, 1173 (2011).

[4] M. Hermele, M. P. A. Fisher, and L. Balents, Phys. Rev. B **69**, 064404 (2004).

[5] S. V. Isakov, Y. B. Kim, and A. Paramekanti, Phys. Rev. Lett. **97**, 207204 (2006).

[6] A. Banerjee, S. V. Isakov, K. Damle, and Y. B. Kim, Phys. Rev. Lett. **100**, 047208 (2008).

[7] S. V. Isakov, M. B. Hastings, and R. G. Melko, Nat. Phys., doi: 10.1038/nphys2036 (2011).

[8] R. Moessner and K. S. Raman, in *Introduction to Frustrated Magnetism: Materials, Experiments, Theory*, edited by C. Lacroix, F. Mila, and P. Mendels (Springer, Berlin, 2011).

[9] O. Sikora, F. Pollmann, N. Shannon, K. Penc, and P. Fulde, Phys. Rev. Lett. **103**, 247001 (2009).

[10] R. Moessner and S. L. Sondhi, Phys. Rev. Lett. **86**, 1881 (2001).

[11] R. Moessner and S. L. Sondhi, Phys. Rev. B **63**, 224401 (2001).

[12] B. K. Chakrabarti, A. Dutta, and P. Sen, *Quantum Ising Phases and Transitions in Transverse Field Ising Models* (Springer, Berlin, 1996).

[13] E. H. Lieb, Phys. Rev. **162**, 162 (1967).

[14] A. H. Castro Neto, P. Pujol, and E. Fradkin, Phys. Rev. B **74**, 024302 (2006).

[15] R. Moessner, O. Tchernyshyov, and S. Sondhi, J. Stat. Phys. **116**, 755 (2004).

[16] N. Shannon, G. Misguich, and K. Penc, Phys. Rev. B **69**, 220403(R) (2004).

[17] Y. Zhou, Phys. Rev. B **72**, 205116 (2005).

[18] A. Ralko, F. Trousselet, and D. Poilblanc, Phys. Rev. Lett. **104**, 127203 (2010).

[19] A. B. Harris, C. Kallin, and A. J. Berlinsky, Phys. Rev. B **45**, 2899 (1992).

[20] J. T. Chalker, P. C. W. Holdsworth, and E. F. Shender, Phys. Rev. Lett. **68**, 855 (1992).

[21] I. Ritchey, P. Chandra, and P. Coleman, Phys. Rev. B **47**, 15342 (1993).

[22] S. E. Korshunov and B. Douçot, Phys. Rev. Lett. **93**, 097003 (2004).

[23] S. E. Korshunov, Phys. Rev. B **71**, 174501 (2005); Phys. Rev. Lett. **94**, 087001 (2005).

[24] C. L. Henley, Phys. Rev. Lett. **96**, 047201 (2006).

[25] T. Coletta, J.-D. Picon, S. E. Korshunov, and F. Mila, Phys. Rev. B **83**, 054402 (2011).

[26] E. Müller-Hartmann and A. Reischl, Eur. Phys. J. B **28**, 173 (2002).

[27] G. Misguich and F. Mila, Phys. Rev. B **77**, 134421 (2008).

[28] T. Holstein and H. Primakoff, Phys. Rev. **58**, 1098 (1940).

[29] L.-P. Henry and T. Roscilde (unpublished).

[30] C. Castelnovo, R. Moessner, and S. L. Sondhi, Nature (London) **451**, 42 (2008).

[31] T. Coletta, N. Laflorencie, and F. Mila, e-print arXiv:1112.5586.

[32] H. W. J. Blöte and Y. Deng, Phys. Rev. E **66**, 066110 (2002).

[33] R. F. Wang, C. Nisoli, R. S. Freitas, J. Li, W. McConville, B. J. Cooley, M. S. Lund, N. Samarth, C. Leighton, V. H. Crespi, and P. Schiffer, Nature (London) **439**, 303 (2006).

[34] D. Gatteschi, R. Sessoli, and J. Villain, *Molecular Nanomagnets* (Oxford University Press, Oxford, UK, 2006).

[35] M. Mannini, F. Pineider, P. Sainctavit, C. Danieli, E. Otero, C. Sciancalepore, A. M. Talarico, M.-A. Arrio, A. Cornia, D. Gatteschi, and R. Sessoli, Nat. Mater. **8**, 194 (2009).

[36] A. Friedenauer, H. Schmitz, J. Glückert, D. Porras, and T. Schätz, Nat. Phys. **4**, 757 (2008).

[37] K. Kim, M.-S. Chang, S. Korenblit, R. Islam, E. E. Edwards, J. K. Freericks, G.-D. Lin, L.-M. Duan, and C. Monroe, Nature (London) **465**, 590 (2010).

[38] R. Islam, E. E. Edwards, K. Kim, S. Korenblit, C. Noh, H. Carmichael, G.-D. Lin, L.-M. Duan, C.-C. Joseph Wang, J. K. Freericks, and C. Monroe, Nat. Commun. **2**, 377 (2011).

[39] R. Schmied, J. H. Wesenberg, and D. Leibfried, Phys. Rev. Lett. **102**, 233002 (2009).

[40] E. R. Mucciolo, A. H. Castro Neto, and C. Chamon, Phys. Rev. B **69**, 214424 (2004).

[41] S. Wessel and I. Milat, Phys. Rev. B **71**, 104427 (2005).

[42] J.-P. Blaizot and G. Ripka, *Quantum Theory of Finite Systems* (MIT Press, Cambridge, MA, 1985).